AIP | Journal of Applied Physics

Continuous current and surface potential models for undoped and lightly doped double-gate metal-oxide-semiconductor field-effect transistors

Hamdy Abd Elhamid and M. J. Deen

Citation: J. Appl. Phys. **103**, 114501 (2008); doi: 10.1063/1.2937177
View online: http://dx.doi.org/10.1063/1.2937177
View Table of Contents: http://jap.aip.org/resource/1/JAPIAU/v103/i11
Published by the AIP Publishing LLC.

Continuous current and surface potential models for undoped and lightly doped double-gate metal-oxide-semiconductor field-effect transistors

Hamdy Abd Elhamid and M. J. Deen[a)]
Electrical and Computer Engineering Department (CRL 226), McMaster University, Hamilton, Ontario L8S 4K1, Canada

(Received 29 January 2008; accepted 29 March 2008; published online 4 June 2008)

We have introduced a continuous, explicit, surface potential model for symmetric undoped and lightly doped double gate metal-oxide-semiconductor field-effect transistor devices. The surface potential model considered both hole and electron quasi-Fermi potential effects. An explicit current model has been introduced in terms of both source and drain charge densities at which hole and electron quasi-Fermi level or IMREFs are defined. The introduced models are directly related to the device biasing and device structure without the need for fitting parameters. Both of the surface potential and current models are continuous from below to above threshold and from linear to saturation of operation regimes. Good agreement has been obtained when our analytical models are compared to numerical results. The effects of hole IMREF on the small-signal (or ac) parameters are also reported. We predicted that the presence of holes has raised the saturation voltage. Also, we have observed from the gate capacitance curve that the hole IMREF should be taken into our account for low frequency applications. © *2008 American Institute of Physics*.
[DOI: 10.1063/1.2937177]

I. INTRODUCTION

The double-gate (DG) architecture is one of the metal-oxide-semiconductor field-effect transistor (MOSFET) structures with a very high potential for scaling to dimensions below 45 nm (Ref. 1) according to the requirements of the silicon roadmap in 2016 (Ref. 2) and beyond. The use of undoped body results in enhanced mobility by eliminating the charge-impurity scattering and reduced parameter variation by eliminating the statistical fluctuation of the dopant concentration.[3] Analytical DG MOSFET charge-voltage models have been proposed.[3–9] However, most of the presented models have neglected the effects of the hole quasi-Fermi potential, i.e., the devices have been considered as N doped with small N_A value which are termed lightly doped.[3–7] The quasi-Fermi potential (or IMREF) is the difference between the electron Fermi potential E_{Fn} and the hole Fermi potential E_{Fp}. This potential was considered previously as the difference between the electron quasi-Fermi potential and the intrinsic quasi-Fermi potential, E_i (i.e., $E_{Fp} \rightarrow E_i$). This assumption is valid for the DG MOSFET capacitor (where there is no applied voltages) and/or closer to the source end. This assumption will no longer be valid when applying a high drain-source voltage V_{ds}, and/or close to the drain end.

At the drain end, the saturation velocity condition occurs and the holes will strongly affect the device performance. From the drain end towards the source end, this effect will be decreased, as already shown from numerical simulation results in Ref. 10 For the pure Si body, the quasi-Fermi potential along the channel thickness is equally splitted around the intrinsic Fermi potential E_i, and for very long channel devices, this potential assumed to be constant along the channel length. Therefore, when considering the device as undoped, both the hole and electron Fermi potentials should be taken into account.

Previously, the electrostatics of DG MOSFET capacitors have been discussed by many authors. In Refs. 3 and 4, the electrostatics of DG MOS devices were studied by considering only the effects of electrons; the hole quasi-Fermi potential was neglected. In Ref. 9 the authors solved the Poisson equation by including both the hole and electron Fermi potentials but after they dropped the effect of holes in their formulation. The surface potential was discussed in Ref. 7 but only the effects of electrons were considered in Poisson's equation. The model in Ref. 7 was updated in Ref. 8 to include the hole effects, but then the authors considered the hole Fermi potential as a reference potential, this leading to the same formulation as in the previous predictions. An advantage of that model[8] was the introduction of an empirical expression for the surface potential in terms of the electric field. Most of the previous publications showed very good agreement between analytical predictions and the numerical results in which the holes are neglected in DG MOSFET capacitors. In this work, we will introduce different models for the surface potential that includes both holes and electrons. We solved the one dimensional (1D) Poisson equation for symmetric DG MOSFETs at which the electron and hole Fermi potentials are included.

All results in this work have been obtained at room temperature. The other device details used are midgap work function, channel length of 1 μm, channel thickness of 20 nm, oxide thickness of 2 nm, saturation velocity of 7×10^6 cm/s, and low-field mobility of 300 $\mathrm{cm}^2/\mathrm{V\,s}$. At some situations, we have used a different channel length, channel thickness, and effective mobility and it will be indicated through the figure labels. Through this work, some curves

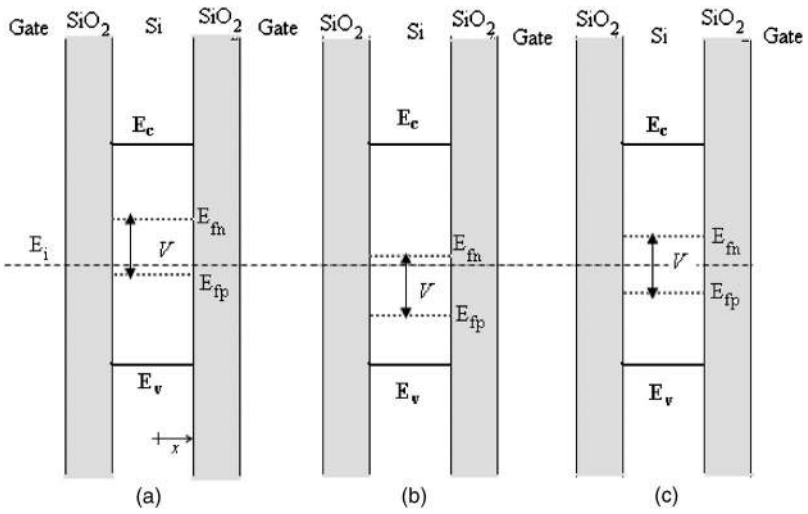

FIG. 1. Band structure diagram at the equilibrium of DG MOSFET at different situations: (a) hole IMREF =0, (b) electron IMREF=0, and (c) $E_{Fn}=-E_{Fp}=V/2$.

(for the electrostatic potential/charge) have been drawn at certain quasi-Fermi potential value, V; this value means at any arbitrary position along the channel length (where the quasi-Fermi potentials have different values along the channel length).

This paper is organized as follows. In sec. II, a surface potential model in terms of the center potential is introduced, and it is verified with published results. We also discuss the drain current that is obtained by direct integration of the charge over the channel. In Sec. III, empirical surface and center potential models in terms of drain and source charge densities is introduced and discussed. A compact current model also will be introduced in Sec. IV in terms of source and drain charge densities. Also, an important physics (which includes both holes and electrons) will be introduced in Sec. IV Summary and conclusion will be finally introduced in Sec V.

II. AN IMPLICIT SURFACE POTENTIAL MODEL

The devices with undoped body are those in which $N_D(x)=N_A(x)=0$ (there are neither acceptor atoms nor donor atoms). The 1D Poisson equation will have the mobile charge only and can be written as

$$\frac{d^2\phi(x)}{dx^2} = -\frac{q}{\varepsilon_s}[n(x)-p(x)] = \frac{q}{\varepsilon_s}[p(x)-n(x)]. \tag{1}$$

The quasi-Fermi potential along the channel depth is defined as the difference between the hole and electron quasi-Fermi potentials, or

$$\phi_{Fn}-\phi_{Fp}=V. \tag{2}$$

Here the intrinsic Fermi potential is considered as a reference bias (zero reference). For the undoped devices or for lightly N-doped devices, if the hole IMREF has been neglected (i.e., the hole Fermi potential E_{Fp} close to the intrinsic Fermi potential E_i), then Eq. (2) can be written as

$$\phi_{Fn}=V. \tag{3}$$

For the same situation for the undoped devices or for lightly P-doped devices if the electron IMREF has been neglected (i.e., the electron Fermi potential E_{Fn} close to the intrinsic Fermi potential E_i), Eq. (2) can be written as

$$\phi_{Fp}=-V. \tag{4}$$

To study the hole effect on the undoped or lightly doped N type, we define

$$\phi_{Fn}=\alpha V, \tag{5}$$

$$\phi_{Fp}=(\alpha-1)V. \tag{6}$$

Here α is a unitless parameter and $(\phi_{Fn}\rightarrow 0)0\leqslant\alpha\leqslant 1(\phi_{Fp}\rightarrow 0)$. The value of α is related to the dopant concentrations and the temperature.

Setting Eqs. (5) and (6) into Eq. (2), we get

$$(\phi_{Fn}-\phi_{Fp})=[\alpha V-(\alpha-1)V]=V. \tag{7}$$

Equation (7) is valid for any given value of α. When neglecting the effect of holes by setting $\alpha=1$ in Eq. (7), the device is lightly N doped [see Fig. 1(a)]. In this case, the carrier density becomes

$$n(x)=\frac{q}{\varepsilon_s}n_i(e^{[\phi(x)-V]/V_{\text{th}}}-e^{-\phi(x)/V_{\text{th}}}). \tag{8}$$

When neglecting the effect of electrons by setting $\alpha=0$ in Eq. (7), the device is lightly P doped [see Fig. 1(b)]. In this case, the carrier density becomes

$$n(x)=\frac{q}{\varepsilon_s}n_i(e^{\phi(x)/V_{\text{th}}}-e^{-[\phi(x)-V]/V_{\text{th}}}). \tag{9}$$

For the pure or intrinsic Si, $\alpha=0.5$ [see Fig. 1(c)], so

$$n(x)=\frac{q}{\varepsilon_s}n_i(e^{(\phi(x)-0.5V)/V_{\text{th}}}-e^{-(\phi(x)-0.5V)/V_{\text{th}}}). \tag{10}$$

From Eqs. (8)–(10), we have, in general,

$$n(x)=\frac{q}{\varepsilon_s}(n_ie^{(\phi(x)-\alpha V)/V_{\text{th}}}-n_ie^{[(\alpha-1)V-\phi(x)]/V_{\text{th}}}). \tag{11}$$

Setting Eq. (11) into Eq. (1), Poisson's equation can then be written as

$$\frac{d^2\phi(x)}{dx^2} = \frac{q}{\varepsilon_s}(n_i e^{(\phi(x)-\alpha V)/V_{\text{th}}} - n_i e^{[(\alpha-1)V-\phi(x)]/V_{\text{th}}})$$

$$= \frac{q}{\varepsilon_s} n_i e^{-V/2V_{\text{th}}}(e^{[\phi(x)-(\alpha-0.5)V]/V_{\text{th}}} - e^{-[\phi(x)-(\alpha-0.5)V]/V_{\text{th}}}) \text{ or}$$

$$\frac{d^2\phi(x)}{dx^2} = 2\frac{q}{\varepsilon_s} n_i e^{-V/2V_{\text{th}}} \sinh\left(\frac{\phi(x)-(\alpha-0.5)V}{V_{\text{th}}}\right). \quad (12)$$

For simplicity, we define $\beta=(\alpha-0.5)$, so we have $(\phi_{Fn} \rightarrow 0)-0.5 \leqslant \beta \leqslant 0.5(\phi_{Fp} \rightarrow 0)$. Rewriting Eq. (12) in terms of β instead of α, we get

$$\frac{d^2\phi(x)}{dx^2} = 2\frac{q}{\varepsilon_s} n_i e^{-V/2V_{\text{th}}} \sinh\left(\frac{\phi(x)-\beta V}{V_{\text{th}}}\right). \quad (13)$$

Now, multiplying Eq. (13) by $d\phi$ and integrating once,

$$\left\{\frac{d\phi(x)}{dx}\right\}^2 - \left(\frac{d\phi(x)}{dx}\right)^2\Big|_{x=0} = k_2^2\left\{\cosh\left(\frac{\phi(x)-\beta V}{V_{\text{th}}}\right) - \cosh\left(\frac{\phi_0-\beta V}{V_{\text{th}}}\right)\right\}, \quad (14)$$

$$k_2 = \sqrt{\frac{4qn_i V_{\text{th}}}{\varepsilon_s} e^{V/2V_{\text{th}}}}. \quad (15)$$

ϕ_0 is the potential at the center of the body. From device symmetry, ; $d\phi(x)/dx|_{x=0}=0$, so Eq. (14) becomes

$$E(x) = \frac{d\phi(x)}{dx} = k_2\sqrt{\left\{\cosh\left(\frac{\phi(x)-\beta V}{V_{\text{th}}}\right) - \cosh\left(\frac{\phi_0-\beta V}{V_{\text{th}}}\right)\right\}}. \quad (16)$$

The surface electric field E_s can be found from Eq. (16) by setting $x=T_{si}/2$,

$$E_s = k_2\sqrt{\left[\cosh\left(\frac{\phi_s-\beta V}{V_{\text{th}}}\right) - \cosh\left(\frac{\phi_0-\beta V}{V_{\text{th}}}\right)\right]}. \quad (17)$$

Here ϕ_s and ϕ_0 are the surface and center potentials. We have followed the same procedures in Ref. 7 to integrate Eq. (16). The surface potential is then found as

$$\phi_s = V_{\text{th}}\cosh^{-1}\left[\cosh\left(\frac{\phi_0-\beta V}{V_{\text{th}}}\right) \times\left\{1+\tan^2\left[k_3\sqrt{\cosh\left(\frac{\phi_0-\beta V}{V_{\text{th}}}\right)}\right]\right\}\right] + \beta V, \quad (18)$$

with

$$k_3 = \left(\frac{T_{si}}{4V_{\text{th}}}\right)k_2. \quad (19)$$

The boundary condition at the oxide-semiconductor interface is

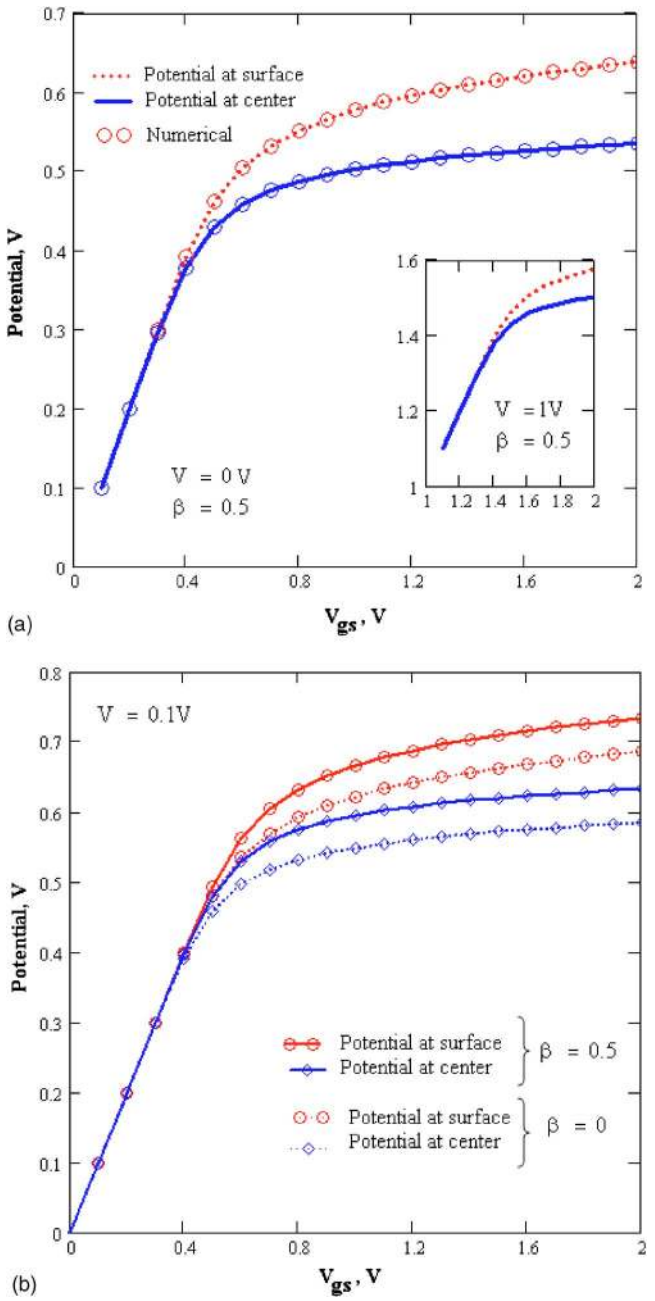

FIG. 2. (Color online) Surface and center potentials at (a) lightly *N*-doped devices (electrons only), and (b) undoped (dotted lines) and lightly doped *N* devices (solid line).

$$C_{\text{ox}} \times (V_{gs} - V_{\text{fb}} - \phi_s) = \varepsilon_s E_s. \quad (20)$$

In Eq. (20), V_{fb}, ε_s, and C_{ox} are the flat band voltage, silicon dielectric constant, and gate capacitance per unit area $(\varepsilon_{\text{ox}}/t_{\text{ox}})$, respectively. Then setting Eqs. (17) and (18) into Eq. (20), we can find the center potential and the surface potential.

Figure 2 shows the iterative solution of both the surface, and center potentials with good agreement with the numerical simulation results. In Fig. 2(a), we have ignored the hole effects, i.e., $\beta=0.5$. In Fig. 2(b), we have considered both hole and electron quasi-Fermi potentials for $\beta=0$, $[V=\phi_{Fn}-\phi_{Fp}=(V/2)-(-V/2)=V]$.

The quasi-Fermi potential effect will appear at any ap-

plied biasing. This effect (splitting) can be ignored at the source end ($V=V_s\rightarrow 0$) and will be extremely high at the drain end ($V=V_{ds}$). For any applied drain to source voltage, the hole quasi-Fermi potential cannot be ignored [see Eq. (7), $\alpha V-(\alpha-1)V\neq\alpha V$ if $\alpha\neq 1$] at the drain end. For undoped devices, the hole quasi-Fermi potential $[(\alpha-1)V]$ will have a strong effect on the drain current, especially at saturation conditions ($V=V_{ds\text{-sat}}$). To overcome the quasi-Fermi potential splitting effects, the quantity $\phi(x)/V_{\text{th}}$ should be much higher than V/V_{th}.

From the surface potential [Eq. (18)], the drain current can be calculated directly by integrating the inversion density charge Q_i from the source to the drain,

$$Q_i = 2\varepsilon_s E_s. \tag{21}$$

Note that the factor of 2 in Eq. (21) is due to the top and bottom gates. Now, assuming a gradual-channel approximation, we get

$$I_{ds} = \mu\frac{W}{L}\int_0^{V_{ds}} Q_i(V)dV. \tag{22}$$

Figure 3 shows the drain current obtained from Eq. (22), but the effects of holes are neglected, i.e., $\beta=0.5$. As shown in Figs. 3(a) and 3(b), there is good agreement between calculations using Eq. (22) and the numerical simulation results.

The surface potential can be refined by trying to solve the last three equations, Eqs. (17), (18), and (20), together to get a closed form solution instead of solving the surface potential iteratively. Equation (20) can be written as

$$V_{gs}-V_{\text{fb}}-\phi_s = \frac{\varepsilon_s}{C_{\text{ox}}}E_s. \tag{23}$$

Now, substituting Eq. (17) into Eq. (23), we get

$$V_{gs}-V_{\text{fb}} = \phi_s + \frac{\varepsilon_s}{C_{\text{ox}}}k_2\sqrt{\cosh\left(\frac{\phi_s-\beta V}{V_{\text{th}}}\right)-\cosh\left(\frac{\phi_0-\beta V}{V_{\text{th}}}\right)}, \tag{24}$$

$$V_{gs}-V_{\text{fb}} \approx \phi_s + \frac{\varepsilon_s}{C_{\text{ox}}}k_2\exp\left(\frac{\phi_s-\beta V}{2V_{\text{th}}}\right)\sqrt{1-\exp\left(\frac{\phi_0-\phi_s}{V_{\text{th}}}\right)}. \tag{25}$$

From Eq. (18), we can write

$$\cosh\left(\frac{\phi_s-\beta V}{V_{\text{th}}}\right) = \cosh\left(\frac{\phi_0-\beta V}{V_{\text{th}}}\right)\times\left\{1+\tan^2\left[\sqrt{k_3{}^2\cosh\left(\frac{\phi_0-\beta V}{V_{\text{th}}}\right)}\right]\right\} \tag{26}$$

or

$$\frac{\cosh\left(\frac{\phi_s-\beta V}{V_{\text{th}}}\right)}{\cosh\left(\frac{\phi_0-\beta V}{V_{\text{th}}}\right)} = \sec^2\left[\sqrt{k_3{}^2\cosh\left(\frac{\phi_0-\beta V}{V_{\text{th}}}\right)}\right], \tag{27}$$

$$\frac{\cosh\left(\frac{\phi_0-\beta V}{V_{\text{th}}}\right)}{\cosh\left(\frac{\phi_s-\beta V}{V_{\text{th}}}\right)} = \cos^2\left[\sqrt{k_3{}^2\cosh\left(\frac{\phi_0-\beta V}{V_{\text{th}}}\right)}\right], \tag{28}$$

$$\cos^2\left[\sqrt{k_3{}^2\cosh\left(\frac{\phi_0-\beta V}{V_{\text{th}}}\right)}\right] = \exp\left(\frac{\phi_0-\phi_s}{V_{\text{th}}}\right)\times\left[\frac{1+\exp\left(-2\frac{\phi_0-\beta V}{V_{\text{th}}}\right)}{1+\exp\left(-2\frac{\phi_s-\beta V}{V_{\text{th}}}\right)}\right], \tag{29}$$

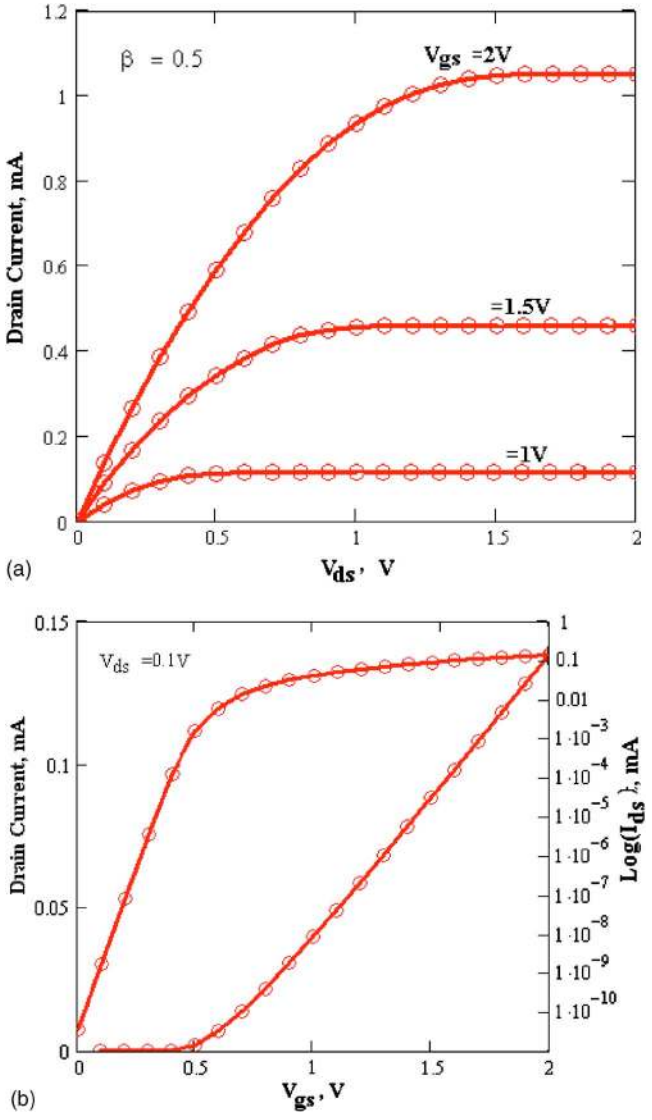

FIG. 3. (Color online) The drain current vs (a) drain-source voltage at different gate-source voltages, and (b) gate-source voltage for linear and logarithmic scales at $V_{ds}=0.1$ V. The circle symbols are the numerical simulation results.

$$\cos^2\left[\sqrt{k_3{}^2\cosh\left(\frac{\phi_0-\beta V}{V_{\text{th}}}\right)}\right]\approx\exp\left(\frac{\phi_0-\phi_s}{V_{\text{th}}}\right). \tag{30}$$

Now, let

$$\cos^2[\eta]=\exp\left(\frac{\phi_0-\phi_s}{V_{\text{th}}}\right), \tag{31}$$

where

$$\eta=\sqrt{k_3{}^2\cosh\left(\frac{\phi_0-\beta V}{V_{\text{th}}}\right)}. \tag{32}$$

Then, setting Eq. (31) into Eq. (25), we get

$$V_{gs}-V_{\text{fb}}=\phi_s+\frac{\varepsilon_s}{C_{\text{ox}}}k_2\exp\left(\frac{\phi_s-\beta V}{2V_{\text{th}}}\right)\sqrt{1-\cos^2[\eta]} \tag{33}$$

since

$$\sin[\eta]=\sqrt{1-\cos^2[\eta]}. \tag{34}$$

Then, setting Eq. (34) into Eq. (33), we get

$$V_{gs}-V_{\text{fb}}=\phi_s+\frac{\varepsilon_s}{C_{\text{ox}}}k_2\exp\left(\frac{\phi_s-\beta V}{2V_{\text{th}}}\right)\sin[\eta] \tag{35}$$

or

$$\phi_s=V_{gs}-V_{\text{fb}}-2V_{\text{th}}W\left[\frac{\varepsilon_s}{2V_{\text{th}}C_{\text{ox}}}k_2\sin[\eta]\exp\left(\frac{V_{gs}-V_{\text{fb}}-\beta V}{2V_{\text{th}}}\right)\right]. \tag{36}$$

In Eq. (36), W is the Lambert function. Note that Eq. (36) will tend to the model presented in Ref. 9 at $\exp[-(\phi_0-\beta V)/V_{\text{th}}]\approx 0$, that is, when the effect of holes are neglected, or

$$E_s=k_2\sqrt{\cosh\left(\frac{\phi_0-\beta V}{V_{\text{th}}}\right)\left[1+k_3{}^2\cosh\left(\frac{\phi_0-\beta V}{V_{\text{th}}}\right)\right]-\cosh\left(\frac{\phi_0-\beta V}{V_{\text{th}}}\right)}, \tag{40}$$

or

$$E_s=k_2\sqrt{k_3{}^2\left[\cosh\left(\frac{\phi_0-\beta V}{V_{\text{th}}}\right)\right]^2}, \tag{41}$$

or

$$E_s=k_4\cosh\left(\frac{\phi_0-\beta V}{V_{\text{th}}}\right),\quad \text{where } k_4=k_2k_3. \tag{42}$$

The charge can be written as

$$Q=\varepsilon_sE_s. \tag{43}$$

Substituting Eq. (42) into Eq. (43),

$$\eta=\sqrt{k_3{}^2\cosh\left(\frac{\phi_0-\beta V}{V_{\text{th}}}\right)}\approx\sqrt{0.5k_3{}^2\exp\left(\frac{\phi_0-\beta V}{V_{\text{th}}}\right)}. \tag{37}$$

Also, Eq. (36) is considered as a general solution for the surface potential in terms of the Lambert function.

III. A CONTINUOUS SURFACE POTENTIAL MODEL

The surface potential model in Eq. (36) is directly related to the gate-source potential. However, the center potential ϕ_0 should be calculated iteratively or by introducing a smoothing function to obtain the exact value of η. In this section, we shall introduce a new empirical model for the surface potential without introducing any smoothing functions.

The surface potential in Eq. (18) can be written as

$$\phi_s\approx V_{\text{th}}\cosh^{-1}\left[\cosh\left(\frac{\phi_0-\beta V}{V_{\text{th}}}\right)\times\left\{1+\sqrt{k_3{}^2\cosh\left(\frac{\phi_0-\beta V}{V_{\text{th}}}\right)}\right\}^2\right]+\beta V \tag{38}$$

or

$$\cosh\left(\frac{\phi_s-\beta V}{V_{\text{th}}}\right)=\cosh\left(\frac{\phi_0-\beta V}{V_{\text{th}}}\right)\left[1+k_3{}^2\cosh\left(\frac{\phi_0-\beta V}{V_{\text{th}}}\right)\right]. \tag{39}$$

Setting Eq. (39) into the electric field surface potential [Eq. (17)], we get

$$Q=\varepsilon_sk_4\cosh\left(\frac{\phi_0-\beta V}{V_{\text{th}}}\right), \tag{44}$$

or

$$\cosh\left(\frac{\phi_0-\beta V}{V_{\text{th}}}\right)=\frac{Q}{\varepsilon_sk_4}. \tag{45}$$

Now, substituting Eq. (45) into Eq. (23) (see the Appendix for details), we get

$$V_{gs}-V_{\text{fb}}-(\beta+0.5)V-V_0=V_{\text{th}}\ln\left[1+2\frac{Q}{Q_0}\right]+V_{\text{th}}\ln\left[\frac{Q}{Q_0}\right]+\frac{Q}{C_{\text{ox}}}, \tag{46}$$

where

$$Q_0 = \left(8\frac{V_{\text{th}}\varepsilon_s}{T_{si}}\right) \tag{47}$$

and

$$V_0 = V_{\text{th}} \ln\left(16\frac{V_{\text{th}}\varepsilon_s}{qn_i T_{si}^{\ 2}}\right). \tag{48}$$

Above the threshold voltage, $Q \gg Q_0$, so the last term in Eq. (46) (i.e., Q/C_{ox}), will be much higher than the logarithmic terms. Therefore, the charge can be written as

$$Q = C_{\text{ox}}[V_{gs} - V_{\text{fb}} - (\beta + 0.5)V - V_0]. \tag{49}$$

On the other hand, below the threshold voltage, $Q \ll Q_0$ (where $\ln[1+2Q/Q_0] \approx \ln[1]=0$), and now the charge can be written as

$$Q = Q_0 e^{[V_{gs}-V_{\text{fb}}-(\beta+0.5)V-V_0]/V_{\text{th}}}. \tag{50}$$

For both regions below and above the threshold voltage, the following empirical expression can be used:[11]

$$Q_c = C_{\text{ox}}\left[-2C_{\text{ox}}\frac{V_{\text{th}}^{\ 2}}{Q_0} + \sqrt{\left(2C_{\text{ox}}\frac{V_{\text{th}}^{\ 2}}{Q_0}\right)^2 + 4V_{\text{th}}^{\ 2}\ln(1+e^{[V_{gs}-V_{\text{fb}}-(\beta+0.5)V-V_0]/2V_{\text{th}})^2}}\right]. \tag{51}$$

The charge model given in Eq. (51) is valid for both regions of operation. From Fig. 4, the charge model given in Eq. (51) results in a charge density that is higher than the iterative solution for the charge density that is given in Eq. (21) in the saturation region.

To correct Eq. (51), let us rewrite Eq. (46) as

$$Q = C_{\text{ox}}\left\{V_{gs} - V_{\text{fb}} - (\beta+0.5)V - V_0 - V_{\text{th}}\ln\left[\frac{Q_c}{Q_0} + 2\left(\frac{Q_c}{Q_0}\right)^2\right]\right\}. \tag{52}$$

Now, from Eq. (52), the threshold voltage can be written as

$$V_T = V_0 + V_{\text{th}}\ln\left[\frac{Q_c}{Q_0} + 2\left(\frac{Q_c}{Q_0}\right)^2\right] = V_0 + V_{\text{th}}\ln\left[\frac{Q_c}{Q_0}\right] + V_{\text{th}}\ln\left[1+2\frac{Q_c}{Q_0}\right]. \tag{53}$$

Note that Eq. (53) cannot be used as a universal definition for the threshold voltage because of the infinite value of the logarithmic terms in the subthreshold regime at which the threshold voltage should be V_0 [see Eq. (50)]. We can use the following expression to express the threshold voltage for both regimes (see Fig. 5),

$$V_T = V_0 + 2V_{\text{th}}\ln\left[1+\frac{Q_c}{Q_0}\right]. \tag{54}$$

From Eq. (54), in the subthreshold regime where $Q \ll Q_0$ and $\ln[1+Q_c/Q_0] \to 0$, we get $V_T = V_0$, as expected. In the saturation region where $Q \gg Q_0$ and $2Q_c/Q_0 \approx Q_c/Q_0$, then $V_T = V_0 + 2V_{\text{th}}\ln[1+Q_c/Q_0]$. By using the empirical expression in Ref. 12, instead of Eq. (51),

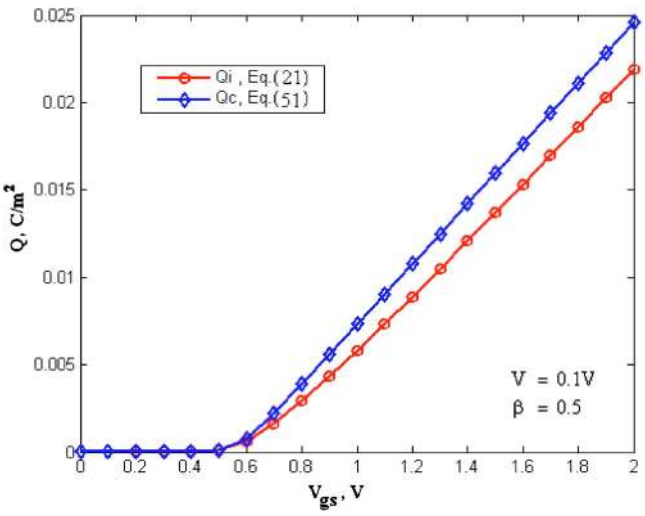

FIG. 4. (Color online) A comparison between the empirical charge expression, Eq. (51), and the iterative solution in Eq. (21) at $V=0.1$ V (at arbitrary channel position).

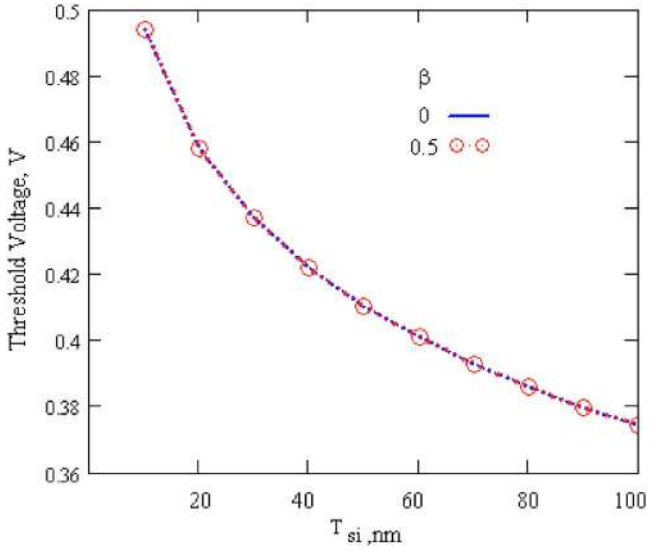

FIG. 5. (Color online) The threshold voltage vs silicon thickness according to Eq. (54).

$$Q = C_{ox}\left[-2C_{ox}\frac{V_{th}^{\ 2}}{Q_0} + \sqrt{\left(2C_{ox}\frac{V_{th}^{\ 2}}{Q_0}\right)^2 + 4V_{th}^{\ 2}\ln(1+e^{[V_{gs}-V_{fb}-(\beta+0.5)V+V_T-\Delta V_T]/2V_{th}})^2}\right]. \quad (55)$$

We note that Q_c in Eq. (51) can be used as a first trial to get the final charge in Eq. (55). Also,

$$\Delta V_T = \frac{2C_{ox}V_{th}^{\ 2}\dfrac{Q_c}{Q_0}}{Q_0+Q_c}, \quad (56)$$

where ΔV_T is added to ensure that the charge will reach its saturation value as given in Eq. (49).

As shown in Fig. 6, very good agreement has been obtained between the final empirical expression given in Eq. (55) and the exact solution in Eq. (21).

After some mathematical manipulations, the potential at the center can be written as (see the Appendix for details),

$$\phi_0 = V_{th}\ln\left[\frac{Q}{Q_0}\right] + (\beta+0.5)V + V_0 \quad (57)$$

and

$$\phi_s = \phi_0 + V_{th}\ln\left[1+2\frac{Q}{Q_0}\right]. \quad (58)$$

Equations (57) and (58) are closed form, compact models for the center and surface potentials, respectively. The potential models of Eqs. (57) and (58) includes the effects of both holes and electrons in terms of the charge.

Figure 7 shows an excellent matching between the introduced models in Eqs. (57) and (58) for both the center and surface potentials, respectively, with the iterative models given in Eq. (18). The difference between the surface and center potentials can be found by subtracting Eq. (57) from Eq. (58),

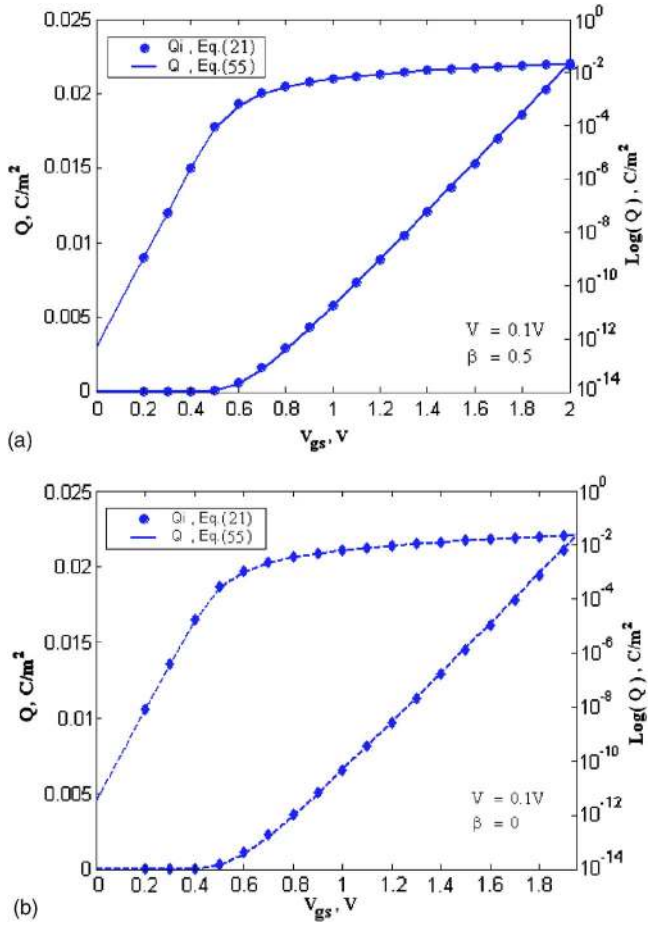

FIG. 6. (Color online) A comparison between the empirical charge expression, Eq. (55), and the iterative solution in Eq. (21) [(a) β=0.5 (neglecting hole effects) and (b) β=0 (hole and electron effects are included)] at V =0.1 V.

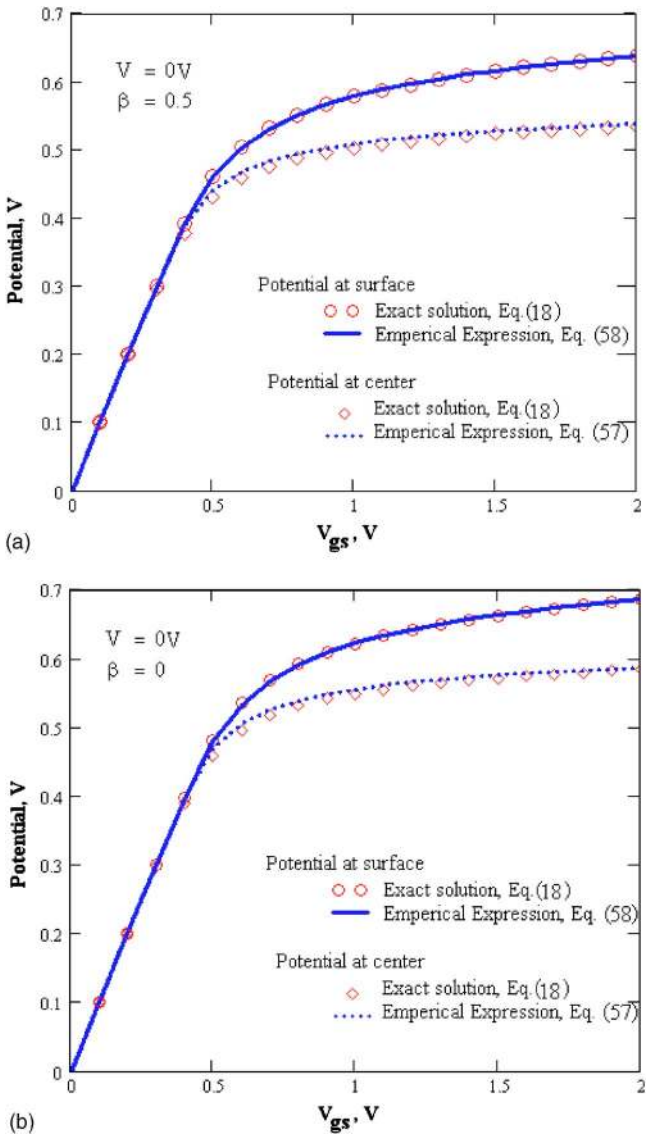

FIG. 7. (Color online) A comparison between the potential expression, Eqs. (57) and (58), and the iterative solution in Eq. (18). (a) β=0.5 (neglecting hole effect) and (b) β=0 (electron and hole effects are included).

$$\phi_s - \phi_0 = V_{\text{th}} \ln\left[1 + 2\frac{Q}{Q_0}\right]. \tag{59}$$

In the subthreshold region, $Q \ll Q_0$, so Eq. (59) will become

$$\phi_s - \phi_0 = 0. \tag{60}$$

In the saturation region, $Q \gg Q_0$, so

$$\phi_s - \phi_0 \approx V_{\text{th}} \ln\left[2\frac{Q_{\text{sat}}}{Q_0}\right] \approx V_{\text{th}} \ln\left[\frac{Q_{\text{sat}}}{Q_0}\right]. \tag{61}$$

Here Q_s and Q_d are the charge densities at the source and at the drain ends of the device, and this can be found from Eq. (55) by setting

$$Q_s = Q(y=0) = Q(V=0)$$

and

$$Q_d = Q(y=L) = Q(V=V_{ds}).$$

From Eq. (52), we can write dv in terms of dQ as

$$-dV = \frac{1}{(\beta+0.5)}\left[\frac{1}{C_{\text{ox}}} + \frac{V_{\text{th}}}{Q} + 2\frac{V_{\text{th}}}{Q_0+2Q}\right]dQ. \tag{62}$$

Now, substituting Eq. (62) into Eq. (59) and completing the integration, we get

$$I_{ds} = \mu\frac{W}{L(\beta+0.5)}\left[\frac{Q_s^2 - Q_d^2}{C_{\text{ox}}} + 4V_{\text{th}}(Q_s - Q_d) + V_{\text{th}}Q_0 \ln\left(\frac{Q_0+2Q_d}{Q_0+2Q_s}\right)\right]. \tag{63}$$

Without the last term of Eq. (63), the current model at $\beta=0.5$ tends to be the same as the model in Refs. 13 and 14 In Ref. 13, it was assumed that $\exp[(\phi_0 - V)/V_{\text{th}}] \ll (\varepsilon_s/t_{si})V_{\text{th}}$, and in Ref. 14, it was assumed that $\alpha \approx -2Q_sV_{\text{th}}/\varepsilon_s t_{si}$ (note that this α is different from the α parameter that we introduced in Sec. II). Very importantly, we have not introduced any approximations or fitting parameters for the current model given by Eq. (63). Moreover the model includes the effects of both electrons and holes and Fig. 8 shows the drain current computed using Eq. (63). Very good agreement has been obtained between calculations using Eq. (63) and numerical simulation results. In Fig. 9, both hole and electron effects are taken into account, i.e., $\beta=0$. Figure 9(a) shows that the drain current at $\beta=0$ (where the quasi-Fermi potential has been divided due to the presence of the holes and the electrons) is higher than the current due to the electron IMREF only (at fixed low-field mobility value). The differences between the currents with electrons only and with both holes and electrons are not only due to the effect of holes but are also due to the quasi-Fermi potential splitting and the fixed low-field mobility value.

The effect of holes in Fig. 9(b) is an increase in the subthreshold swing, as shown more clearly in the inset figure. There have been many studies on how to overcome the quasi-Fermi potential splitting effects [of Fig. 1(c)] on the drain current by considering that potential as a reference bias. [4–12,15]. We shall study this assumption in the next section by doubling the quasi-Fermi potential value from V to 2 V. By doubling the quasi-Fermi potential to 2 V, it is equivalent to having a device lightly doped with a very small hole effect [due to the negative exponential part in the carrier density equation, Eq. (10)]. If we kept the quasi-Fermi potential value V too small (i.e., $V/2 \sim V \rightarrow E_i$), neither the electron nor hole IMREFs affect the device performance, where the gradual-channel approximation will be valid for the whole device length.

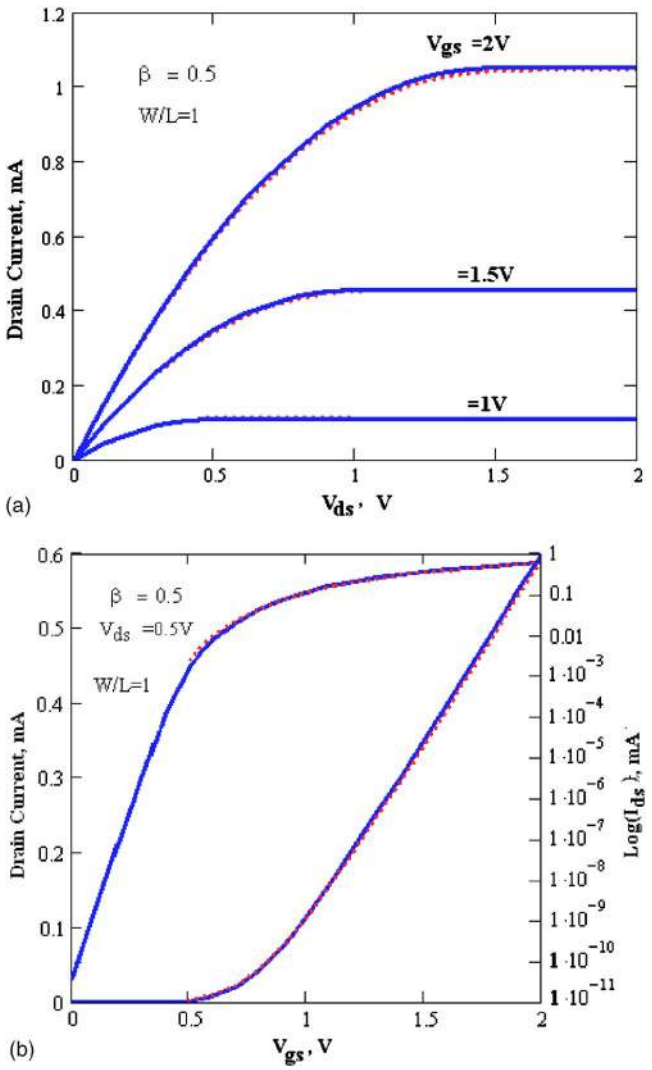

FIG. 8. (Color online) The drain current vs (a) drain-source voltage for different gate-source voltages and (b) gate-source voltage for both linear and logarithmic scales. The solid lines are our model and the dotted lines are numerical results at $\beta=0.5$ (neglecting hole effect).

IV. AC PARAMETERS

To study the quasi-Fermi potential splitting and the effect of holes on the device performance for analog applications, we shall study the channel conductance, transconductance, and gate capacitance.[16] From the continuous current model derived in Eq. (63), the transconductance, g_{ms} can be calculated from

$$g_{ms} \approx \frac{\partial I_{ds}}{\partial V_{gs}}, \tag{64}$$

and the drain conductance can be calculated from

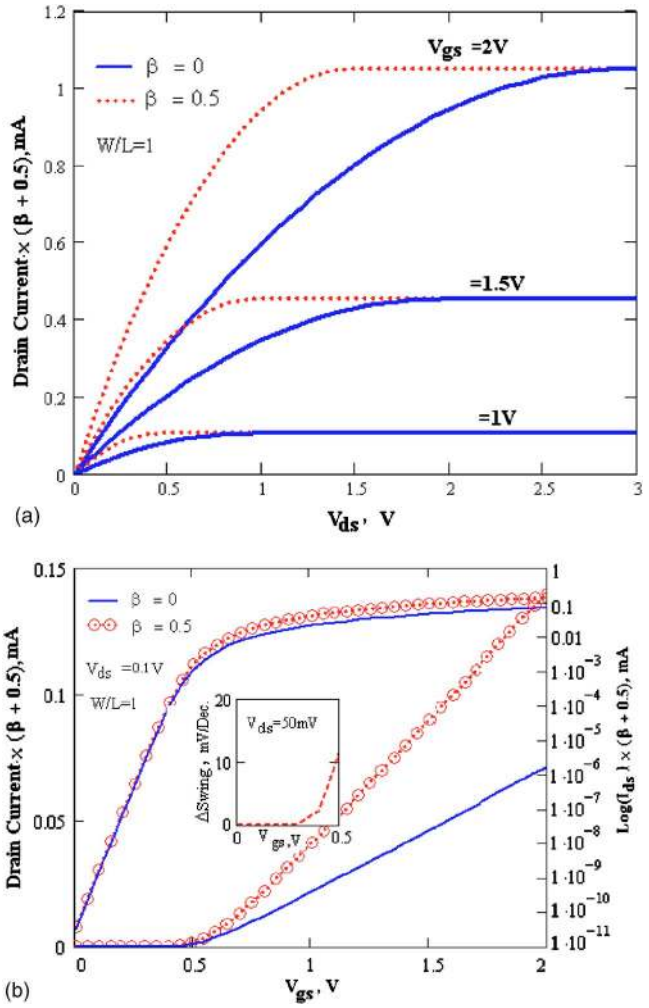

FIG. 9. (Color online) The drain current vs (a) drain-source voltage at different gate-source voltages and (b) gate-source voltage at V_{ds}=0.1 V. The solid lines are at β=0.5, and the dotted lines are at β=0. The inset shows the difference between the subthreshold swing due to two carriers (β=0) and one carrier (β=0.5).

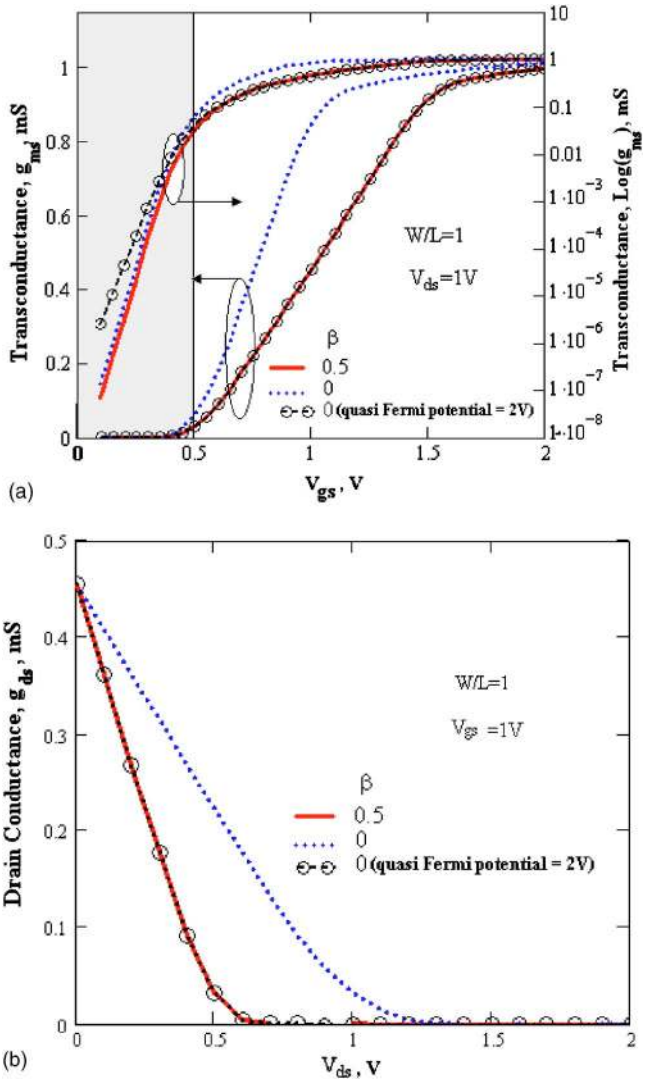

FIG. 10. (Color online) (a) The transconductance vs gate-source voltage (V_{ds}=1 V) and (b) the drain conductance vs drain-source voltage (V_{gs} =1 V). Solid lines at β=0.5 (electrons only), the dot lines at β=0 (quasi-Fermi potential splitting between hole and electron quasi-Fermi potentials), and dotted circled lines at β=0 (quasi-Fermi potential has doubled to 2V).

$$g_{ds} = \frac{\partial I_{ds}}{\partial V_{ds}}. \tag{65}$$

Figures 10(a) and 10(b) show the device transconductance and drain conductance at different situations of hole-electron quasi-Fermi potentials. From Fig. 10(a), the hole quasi-Fermi potential raises the transconductance from the linear to the saturation regimes, and the effect is very small in the subthreshold regime. These changes are not due to the quasi-Fermi potential splitting only, as shown from the logarithmic scale of Fig. 10(b). In Fig. 10(b), we doubled the quasi-Fermi potential to be 2V, instead of V; the holes will strongly affect the device performance in the subthreshold regime [as shown in the shaded region of Fig. 10(a)]. In the strong inversion, the drain conductance with the presence of both holes and electrons will be higher than the drain conductance due to the presence of electrons only. If we have increased the quasi-Fermi potential to 2V instead of V (to ignore the splitting effect), then the effect of holes can be ignored. To conclude, on increasing the quasi-Fermi potential value (can be at the drain end), the effect of holes on the drain conductance and the device transconductance in the saturation regime can be ignored. However, the device transconductance will be strongly affected in below threshold conditions.

Another important parameter is the gate capacitance, and this can be calculated by differentiating the surface charge according to

$$C = \frac{\partial Q}{\partial V_{gs}}. \tag{66}$$

Figure 11 shows the gate capacitance normalized to the oxide capacitance at the quasi-Fermi potential V=0.1 V. As noticed from this figure, there is a relatively high capacitance ratio due to the presence of the holes and electrons (two carriers) compared to the case when no holes are present and at low frequency applications.

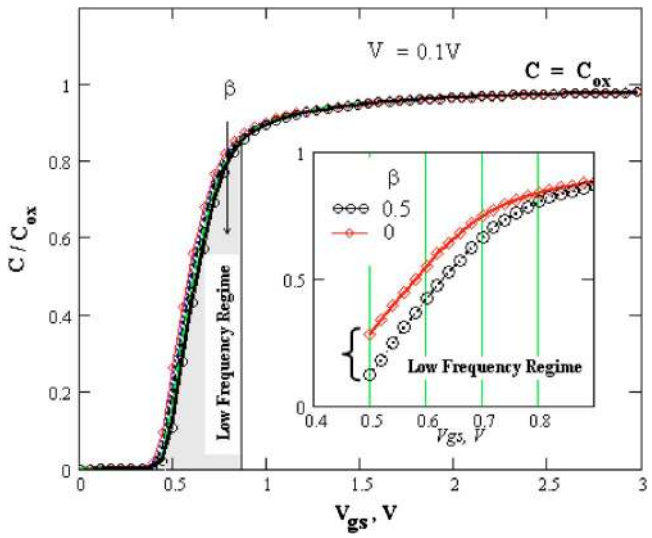

FIG. 11. (Color online) The gate capacitance vs the gate-source voltage at V_{ds}=0.1 V.

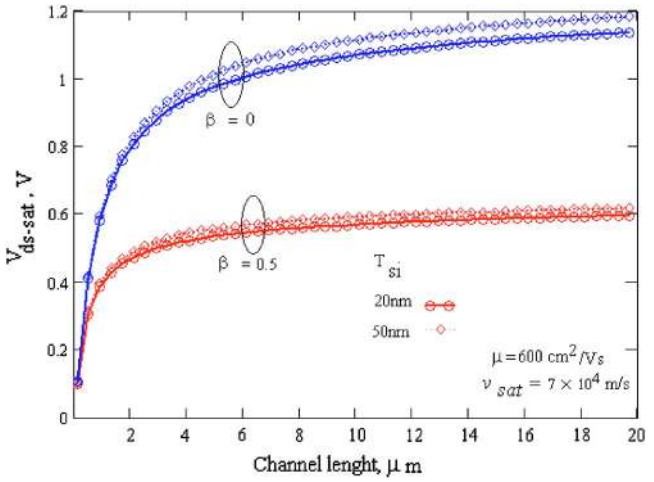

FIG. 12. (Color online) The drain-source saturation voltage at different channel thicknesses vs channel length. For β=0 and 0.5.

Hole IMREF effect on saturation velocity regime

To examine the effect of holes above the threshold voltage, we can explore the velocity saturation region parameters. Note that a compact model for the velocity saturation length is not our objective here. The drain current will be defined as $I_{ds\text{-sat}}$ in this regime of operation and will occur in the region close to the drain end. Also, the electric field will be termed E_{sat}. The saturation drain current can then the written as

$$I_{ds\text{-sat}} = 2\varepsilon_s W E_{\text{sat}} v_{\text{sat}}. \tag{67}$$

Equation (67) can be written in terms of the saturation charge density instead of the saturation electric field and is

$$I_{ds\text{-sat}} = 2WQ_{d\text{-sat}} v_{\text{sat}}. \tag{68}$$

In Eq. (68), $Q_{d\text{-sat}}$ is the charge at which the saturation condition occurs. In the saturation region edge of the device at the drain end where $y=L$, $V=V_{ds\text{-sat}}$ and $Q=Q_{d\text{-sat}}$. The drain current of Eq. (63) can then be written as

$$I_{ds\text{-sat}} = \mu_{\text{eff}} \frac{W}{L(\beta+0.5)} \left[\frac{Q_s^2 - Q_{d\text{-sat}}^2}{C_{\text{ox}}} + 4V_{\text{th}}(Q_s - Q_{d\text{-sat}}) + V_{\text{th}} Q_0 \ln\left(\frac{Q_0 + 2Q_{d\text{-sat}}}{Q_0 + 2Q_s} \right) \right]. \tag{69}$$

By equating Eqs. (68) and (69) for a given V_{gs}, $Q_{d\text{-sat}}$ is evaluated and substituted in the charge equation (55) to obtain "the saturation drain voltage" $V_{ds\text{-sat}}$.

Figure 12 shows that $V_{ds\text{-sat}}$ due to two carriers (electrons and holes) is approximately twice the $V_{ds\text{-sat}}$ due to one carrier (electrons). This difference is a result of the quasi-Fermi potential being split between the hole and electron IMREFs. From Eq. (55), we can write the saturation drain voltage as

$$(\beta+0.5)V_{ds\text{-sat}} = (V_{gs} - V_{\text{fb}} - V_T') - 2V_{\text{th}} \ln\left[e^{\sqrt{\{[Q_{d\text{-sat}}/C_{\text{ox}} + 2C_{\text{ox}}(V_{\text{th}}^2/Q_0)]^2 - [2C_{\text{ox}}(V_{\text{th}}^2/Q_0)]^2\}/4V_{\text{th}}^2}} - 1 \right], \tag{70}$$

with

$$V_T' = \Delta V_T - V_T. \tag{71}$$

To investigate the effect of the holes only on the saturation drain-source voltage $V_{ds\text{-sat}}$, we write

$$\Delta V_{ds\text{-sat}} = V_{ds\text{-sat}}|_{\beta=0.5} - 0.5\, V_{ds\text{-sat}}|_{\beta=0}. \tag{72}$$

Figure 13 shows the effect holes on the saturation drain-source voltage $\Delta V_{ds\text{-sat}}$ according to Eq. (72). Compared to very long channel device lengths, the saturation drain-source voltage due to the presence of holes has been increased by more than 100 mV for channel length devices of lengths down to 1 μm. Note that this difference will be saturated at the thermal voltage value for very long channel devices.

V. CONCLUSIONS

We have introduced a continuous surface potential model for undoped and lightly doped DG MOSFET devices. The model includes both hole and electron quasi-Fermi potentials. The model is continuous from below to above threshold voltage, and from linear to saturation regimes. Also, a continuous current model has been introduced in terms of drain and source charge densities. We have studied the device physics from the output characteristics and some

ac parameters. We have observed that the splitting of the quasi-Fermi potential between the hole and electron IMREFs will introduce a higher drain current in the saturation region. This effect can be ignored if we take the quasi-Fermi potential as a reference bias. We predicted that the presence of holes has raised the saturation voltage by more than 100 mV for a device with channel lengths down to 1 μm. For very long channel length devices, it will be saturated at the thermal voltage value. We have observed from the gate capacitance curve that the hole IMREF should be taken into account for low frequency applications. Also, the holes will raise the subthreshold condition at low drain-source voltage (50 mV) by a value less than 10 mV/Decade.

APPENDIX: DERIVATION OF THE POTENTIAL MODEL

Apply $\cosh^{-1}(x)=\ln[x+\sqrt{x^2-1}]$ to surface potential Eq. (38) to be

$$\phi_s = V_{\text{th}} \ln\left[\cosh\left(\frac{\phi_0-\beta V}{V_{\text{th}}}\right)\left[1+k_3^2\cosh\left(\frac{\phi_0-\beta V}{V_{\text{th}}}\right)\right] \sqrt{\left(\cosh\left(\frac{\phi_0-\beta V}{V_{\text{th}}}\right)\left[1+k_3^2\cosh\left(\frac{\phi_0-\beta V}{V_{\text{th}}}\right)\right]\right)^2-1}\right] + \beta V \tag{A1}$$

or

$$\phi_s = V_{\text{th}} \ln\left[2\cosh\left(\frac{\phi_0-\beta V}{V_{\text{th}}}\right)+2k_3^2\cosh\left(\frac{\phi_0-\beta V}{V_{\text{th}}}\right)^2\right] + \beta V. \tag{A2}$$

From Gauss's law,

$$Q = C_{\text{ox}}[V_{gs}-V_{\text{fb}}-\phi_s] = \varepsilon_s E_s = \varepsilon_s k_4 \cosh\left(\frac{\phi_0-\beta V}{V_{\text{th}}}\right) \tag{A3}$$

or

$$V_{gs}-V_{\text{fb}}-\beta V = V_{\text{th}} \ln\left[2\frac{Q}{\varepsilon_s k_4}+2k_3^2\left(\frac{Q}{\varepsilon_s k_4}\right)^2\right]+\frac{Q}{C_{\text{ox}}}, \tag{A4}$$

$$V_{gs}-V_{\text{fb}}-\beta V = V_{\text{th}} \ln\left[2\frac{Q}{\varepsilon_s k_4}+2\left(k_3\frac{Q}{\varepsilon_s k_4}\right)^2\right]+\frac{Q}{C_{\text{ox}}}, \tag{A5}$$

where

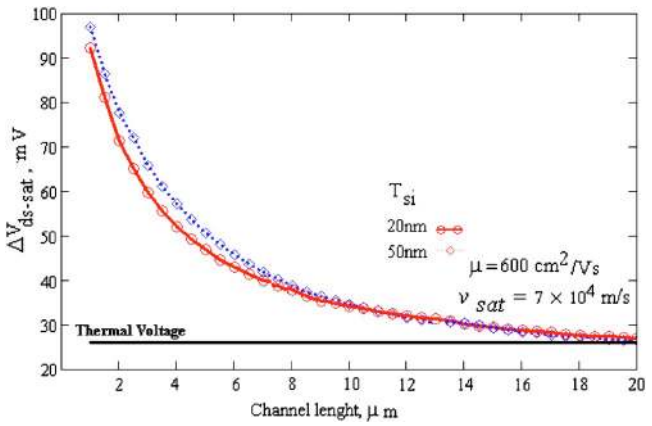

FIG. 13. (Color online) The difference between drain-source saturation voltages vs channel length.

$$\varepsilon_s k_4 = \varepsilon_s k_2 k_3 = \varepsilon_s\left(\frac{T_{si}}{4V_{\text{th}}}\right)k_2^2 = \left(\frac{qn_iT_{si}^2}{8V_{\text{th}}\varepsilon_s}\right)\left(8\frac{V_{\text{th}}}{T_{si}}\varepsilon_s\right)e^{-V/2V_{\text{th}}} \tag{A6}$$

and defining

$$F_0 = \frac{qn_iT_{si}^2}{8V_{\text{th}}\varepsilon_s} \tag{A7}$$

and

$$Q_0 = \left(\frac{8V_{\text{th}}\varepsilon_s}{T_{si}}\right). \tag{A8}$$

Setting Eqs. (A7) and (A8) into Eq. (A6), we get

$$\varepsilon_s k_4 = (Q_0F_0)e^{-V/2V_{\text{th}}}. \tag{A9}$$

Also,

$$\left(\frac{k_3}{\varepsilon_s k_4}\right)^2 = \left(\frac{k_3}{\varepsilon_s k_2 k_3}\right)^2 = \left(\frac{1}{\varepsilon_s k_2}\right)^2 \tag{A10}$$

and

$$(\varepsilon_s k_2)^2 = \varepsilon_s^2\frac{4V_{\text{th}}qn_i}{\varepsilon_s}e^{-V/2V_{\text{th}}} = \frac{1}{2}\left(\frac{qn_iT_{si}^2}{8V_{\text{th}}\varepsilon_s}\right)\times\left(\frac{8V_{\text{th}}\varepsilon_s}{T_{si}}\right)^2 e^{-V/2V_{\text{th}}}. \tag{A11}$$

Setting Eqs. (A7) and (A8) into Eq. (A11), we get

$$(\varepsilon_s k_2)^2 = \frac{Q_0^2F_0}{2}e^{-V/2V_{\text{th}}}. \tag{A12}$$

Substituting Eqs. (A9) and (A12) into Eq. (A5), we obtain

$$V_{gs}-V_{\text{fb}}-\beta V = V_{\text{th}} \ln\left\{2\frac{e^{V/2V_{\text{th}}}}{F_0}\left[\frac{Q}{Q_0}+2\left(\frac{Q}{Q_0}\right)^2\right]\right\} + \frac{Q}{C_{\text{ox}}}, \tag{A13}$$

$$V_{gs} - V_{\mathrm{fb}} - (\beta + 0.5)V - V_{\mathrm{th}} \ln\left(\frac{2}{F_0}\right) = V_{\mathrm{th}} \ln\left[\frac{Q}{Q_0} + 2\left(\frac{Q}{Q_0}\right)^2\right] + \frac{Q}{C_{\mathrm{ox}}}, \tag{A14}$$

or

$$V_{gs} - V_{\mathrm{fb}} - (\beta + 0.5)V - V_{\mathrm{th}} \ln\left(\frac{16V_{\mathrm{th}}\varepsilon_s}{qn_i T_{si}^2}\right) = V_{\mathrm{th}} \ln\left[\frac{Q}{Q_0} + 2\left(\frac{Q}{Q_0}\right)^2\right] + \frac{Q}{C_{\mathrm{ox}}}. \tag{A15}$$

Finally, we can write Eq. (A15) as

$$V_{gs} - V_{\mathrm{fb}} - (\beta + 0.5)V - V_0 = V_{\mathrm{th}} \ln\left[1 + 2\frac{Q}{Q_0}\right] + V_{\mathrm{th}} \ln\left[\frac{Q}{Q_0}\right] + \frac{Q}{C_{\mathrm{ox}}}, \tag{A16}$$

where

$$V_0 = V_{\mathrm{th}} \ln\left(\frac{16V_{\mathrm{th}}\varepsilon_s}{qn_i T_{si}^2}\right). \tag{A17}$$

From Eq. (45), the potential at the body center can be written as

$$\phi_0 = V_{\mathrm{th}} \cosh^{-1}\left[\frac{Q}{\varepsilon_s k_4}\right] + \beta V. \tag{A18}$$

Inserting Eq. (A9) into Eq. (A18),

$$\phi_0 = V_{\mathrm{th}} \cosh^{-1}\left[\frac{Q}{Q_0 F_0} e^{V/2V_{\mathrm{th}}}\right] + \beta V \tag{A19}$$

or

$$\phi_0 = V_{\mathrm{th}} \ln\left[\frac{Q}{Q_0}\right] + (\beta + 0.5)V + V_0. \tag{A20}$$

Substituting Eq. (A20) into Eq. (A2), we get

$$\phi_s = V_{\mathrm{th}} \ln\left[2\cosh\left(\frac{Q}{\varepsilon_s k_4}\right) + 2k_3^2 \cosh\left(\frac{Q}{\varepsilon_s k_4}\right)^2\right] + \beta V. \tag{A21}$$

Setting Eq. (A9) into Eq. (21), we get

$$\phi_s = V_{\mathrm{th}} \ln\left[\frac{Q}{Q_0}\right] + V_{\mathrm{th}} \ln\left[1 + 2\frac{Q}{Q_0}\right] + (\beta + 0.5)V + V_0. \tag{A22}$$

The surface potential can be written in terms of the potential at the center by setting Eq. (A20) into Eq. (A22) to give

$$\phi_s = \phi_0 + V_{\mathrm{th}} \ln\left[1 + 2\frac{Q}{Q_0}\right]. \tag{A23}$$

Subtracting Eq. (A20) from Eq. (A22), we have

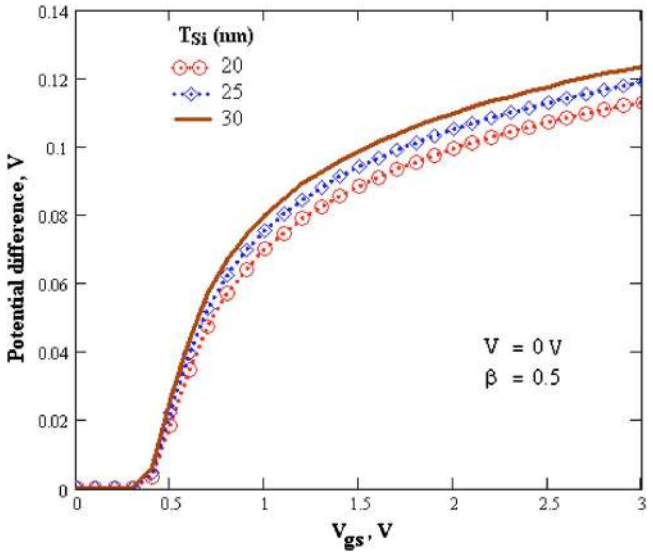

FIG. 14. (Color online) The difference between the surface and center potentials vs gate-source voltage, Eq. (A24).

$$\phi_s - \phi_0 = V_{\mathrm{th}} \ln\left[1 + 2\frac{Q}{Q_0}\right]. \tag{A24}$$

In the subthreshold region, $Q \ll Q_0$, so Eq. (A24) will become (see Fig. 14)

$$\phi_s - \phi_0 = 0. \tag{A25}$$

In the saturation region, $Q \gg Q_0$, so

$$\phi_s - \phi_0 \approx V_{\mathrm{th}} \ln\left[2\frac{Q_{\mathrm{sat}}}{Q_0}\right] \approx V_{\mathrm{th}} \ln\left[\frac{Q_{\mathrm{sat}}}{Q_0}\right] \tag{A26}$$

[1] S.-H. Oh, D. Monroe, and J. M. Hergenrother, IEEE Electron Device Lett. **21**, 445 (2000).
[2] *The International Technology Roadmap for Semiconductors*, 2001 (http://public.itrs.net).
[3] Y. Taur, IEEE Trans. Electron Devices **48**, 2861 (2001).
[4] H. Lu and Y. Taur, IEEE Trans. Electron Devices **53**, 1161 (2006).
[5] X. Zhou, G. H. See, Z. Zhu, S. Lin, C. Wei, G. Zhu, and G. H. Lim, Proceedings of the NSTI Nanotech, Santa Clara, CA, May 2007 (unpublished).
[6] J. He, W. Bian, Y. Tao, F. Liu, K. Lu, W. Wu, T. Wang, and M. Chan, Solid-State Electron. **51**, 179 (2007).
[7] X. Shi and M. Wong, IEEE Trans. Electron Devices **50**, 1793 (2003).
[8] M. Wong and X. Shi, IEEE Trans. Electron Devices **53**, 1389 (2006).
[9] A. Ortiz Conde, F. J. Gracia Sanchez, and S. Malobabic, IEEE Trans. Electron Devices **52**, 1669 (2005).
[10] Q. Chen, E. M. Harrell, and J. D. Miendl, IEEE Trans. Electron Devices **50**, 1631 (2003).
[11] B. Iniguez, L. F. Ferreira, B. Gentinne, and D. Flandre, IEEE Trans. Electron Devices **43**, 568 (1996).
[12] B. Iniguez, D. Jimenez, J. Roig, H. A. Hamid, L. F. Marsal, and J. Pallarès, IEEE Trans. Electron Devices **52**(8), 1868 (2005).
[13] J. He, X. Xi, C. H. Lin, M. Chan, A. Niknejad, and C. Hu, *Proceedings of the Workshop Compact model* (NSTI-Nanotechnology, Boston, MA, 2004).
[14] J. M. Sallese, F. Krummenacher, F. Pregalding, C. llaement, A. Rog, and E. Enz, Solid-State Electron. **49**, 485 (2005).
[15] B. Iñiguez, T. A. Fjeldly, A. Lázaro, F. Danneville, and M. J. Deen, Special Issue on Advanced Compact Models and 45-nm Modeling Challenges [IEEE Trans. Electron Devices **53**, 2128 (2006)].
[16] Y. Cheng, M. J. Deen, and C.-H. Cheng, Special Issue on *Integrated Circuit Technologies for RF Circuit Applications* [Solid-State Electron. **52**, 1286 (2005)].